Research Article Vol. 10, No. 3 / 1 March 2020 / Optical Materials Express 763
Optical Materials EXPRESS

# Influence of process parameters on the incorporation of phosphorus into silica soot material during MCVD process

F. Lindner,[1,*] A. Kriltz,[2] A. Scheffel,[1] A. Dellith,[1] J. Dellith,[1] K. Wondraczek,[1] and H. Bartelt[1]

[1]Leibniz Institute of Photonic Technology, Albert-Einstein-Str. 9, 07745 Jena, Germany
[2]Institute of Physical Chemistry, Friedrich-Schiller-University Jena, Lessingstr. 10, 07743 Jena, Germany
*florian.lindner@leibniz-ipht.de

**Abstract:** The incorporation of phosphorus into silica soot material strongly changes during the multistep preparation process of the MCVD technology in combination with solution doping for Al and rare earths. We report on the influence of various process parameters on the phosphorus concentration, the bond types of phosphorus atoms and the relative density of the soot material. By optimization of the process the phosphorus concentration of the presintered soot could be increased by around 10% in comparison to the conventional treatment. The understanding of the interdependencies allows an improvement of the preparation process of phosphorus co-doped RE doped silica laser fibers with MCVD technology.



## 1. Introduction

Rare earth (RE)-doped fibers with a large-mode area (LMA) structure featuring a large core diameter with a low numerical aperture (NA) enable to achieve high output power in the multi-kW range in fiber lasers or amplifiers. Using phosphorus as co-doping for rare earth doped silica laser fiber materials offer various advantages such as promoting RE-ion solubility in $SiO_2$ matrix, reducing pump induced (photodarkening) losses [1] and enhancing energy transfer from Yb ions to Er ions in Er, Yb-doped laser fibers. The refractive index of the Al/P/RE-doped silica core material as well as photodarkening losses of such fiber can be efficiently reduced with a P/Al-co-doping at a molar ratio of one to one [2,3].

The modified chemical vapor deposition (MCVD) technology in combination with solution doping is the technology of choice for the manufacture of RE-doped high power silica laser fiber preforms [4–6]. The technology is a multistep process involving a deposition of a porous P-doped silica layer, followed by presintering of this layer to a defined relative density $\varphi_{rel}$, a RE/Al solution soaking step of the porous soot layer, drying and cleaning steps followed by a final sintering [7]. The relative density of the porous soot layer compared to the density of the vitrified layer determines the amount of Al and RE, which can be incorporated. A relative density of 0.2 of the porous layer enables sufficient mechanical stability for the subsequent soaking step allowing efficient incorporation of dissolved dopants [6].

However, it is challenging to realize a dip-free refractive index profile with phosphorus co-doping due to evaporation and diffusion of the phosphorus species during the process steps following the solution doping [7,8]. Besides, the chemical nature of incorporated P-species is affected not only by post-soaking steps, but also by deposition and presintering steps prior to solution doping step when the porous P-doped silica soot layer is created.

In phosphosilicate $(P_2O_5)_x(SiO_2)_{1-x}$ glasses tetrahedral silicon-oxygen ($SiO_4$)-groups and phosphorus-oxygen ($O=PO_3$)-groups are randomly distributed in a three-dimensional network.

#385056 https://doi.org/10.1364/OME.385056
Journal © 2020 Received 5 Dec 2019; revised 15 Jan 2020; accepted 15 Jan 2020; published 11 Feb 2020

Optical Materials EXPRESS

Nuclear magnetic resonance (NMR) measurement of silica-phosphate glasses illustrates that phosphorus is entering the silica network only as $Q^3$-group with one P = O-bond [9]. The IR absorption of the Si-O-bonds [10,11] and the P = O-bond [12–15] are well known. Since every P atom of a $(P_2O_5)_x(SiO_2)_{1-x}$ glass is connected within the silica network only as a $Q^3$-group with one P = O-bond, the P = O absorption can be related to the overall phosphorus concentration in the material. Previous FTIR investigations [16] on presintered P-doped silica soot prepared by MCVD process have shown that the P = O band area correlates to the P-concentration of the soot material determined from EDX measurements.

In this work the influence of different process parameters such as sintering temperature and atmospheric conditions of the MCVD solution doping technique on the phosphorus concentration and type of P-related bonds of P-doped silica soot material are evaluated using EDX and FTIR measurements.

## 2. Samples and methods

### 2.1. Sample preparation

Using reverse deposition in the MCVD process, a porous phosphorus doped silica layer was deposited in a silica tube (F300, Heraeus). For the reverse deposition a burner temperature of 1600 °C, a burner velocity of 4 cm/min and a total gas flow of 800 sccm (standard cubic centimeter per minute) were used. The parameters under investigation were as follows: the molar composition of the starting gas phase ($xPOCl_3/xSiCl_4$), the presintering temperature $T_{pre}$ and the presintering atmosphere. Three series of experiments were performed, series A with $xPOCl_3/xSiCl_4 = 0.3$, series B with $xPOCl_3/xSiCl_4 = 0.6$ and series C (varied $xPOCl_3/xSiCl_4$). For comparison only results of a previous work [16] have been added. The samples of series A and series B were first deposited and then presintered either under remaining oxygen gas in the substrate tube or under different gas atmosphere, that is oxygen or helium. In case of presintering without any gas flow a lower presintering temperature was used. The phosphorus doped silica soot layer samples (series C) have been solution doped with pure water by removing 10 - 40 mg of the deposited soot material and mixing it with 4 - 5 ml of pure water. After the standard soaking time of one hour the water was removed and the soot was dried for several days in a desiccator. The P-concentration, the porosity and morphology of the soot samples were characterized using optical microscopy, EDX and ATR-FTIR as described below.

### 2.2. Optical microscopy

The morphological characterization of P-doped soot samples was done on thin segments (length ~ 10 mm) of the silica tube containing the inside-deposited porous layer using an optical microscope (Zeiss microscope Imager M1). The thickness of the porous layer $d_p$ was determined from microscopic images (magnification) at several radial positions. The relative density $\varphi_{rel}$ was then calculated as the ratio of the average measured porous layer thickness $d_p$ over the equivalent thickness of a completely sintered layer $d_s$ (as can be derived from the deposited layer mass) [5]. SEM micrographs were taken using high resolution electron microspcopy (JSM-6300F; JEOL Ltd).

### 2.3. Energy dispersive X-ray spectroscopy (EDX)

Chemical elemental composition of the samples was retrieved using an electron micro probe analyzer JXA-8800L (JEOL Ltd.) equipped with a silicon drift detector XFlash 5010 (Bruker Nano GmbH). A defined amount of the as-deposited soot material was pressed to a thin slice of about two millimeters in diameter directly on an aluminum tube. An evaporated carbon film was used for protection from humidity uptake and charging effects during measurement. Three to five

Optical Materials EXPRESS

samples of every soot material have been prepared. The measurement error for determination of $P_2O_5$ content in those samples is in the range of about 5 - 10%.

### 2.4. Vibrational spectroscopy

Infrared (IR) spectra of the soot samples have been acquired with a FT-IR spectrometer (Nicolet iS10) in attenuated total reflection (ATR) mode in a spectral range from 6000 $cm^{-1}$ to 600 $cm^{-1}$ with a 2 $cm^{-1}$ resolution and an average of 100 scans without advanced ATR correction.

## 3. Results and discussion

### 3.1. Morphology

Previous investigations [7] have shown that the relative density $\varphi_{rel}$ of the porous silica layer determines the efficiency of the incorporation of RE- and Al-ions during the solution doping step. At lower $\varphi_{rel}$ a higher doping level can be achieved, but adhesion of the porous layer to the substrate tube decreased.

Figure 1 shows exemplarily SEM images of the morphology of unsintered and presintered P-doped silica soot material. Through the presintering, the smaller randomly crosslinked structures of the previously unsintered soot grow larger and aligned which led to a more dense structure.

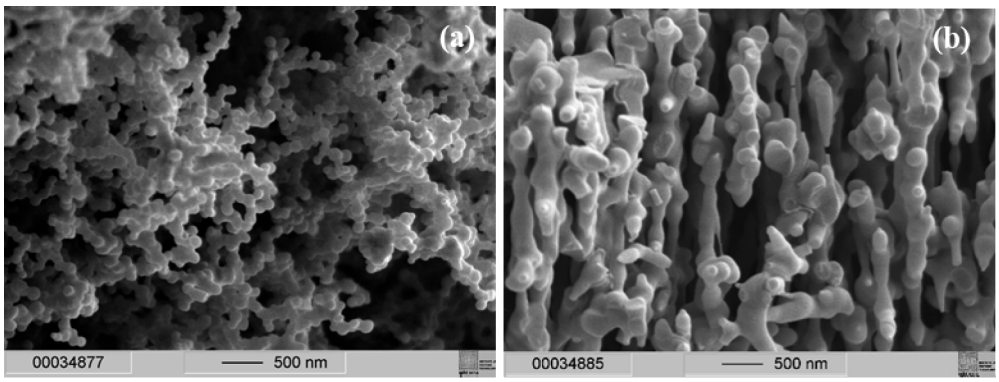


**Fig. 1.** SEM micrographs of unsintered (a) and presintered (b) P-doped silica soot material ($xPOCl_3/xSiCl_4 = 0.6$, $T_{pre} = 1000$ °C, oxygen atmosphere).

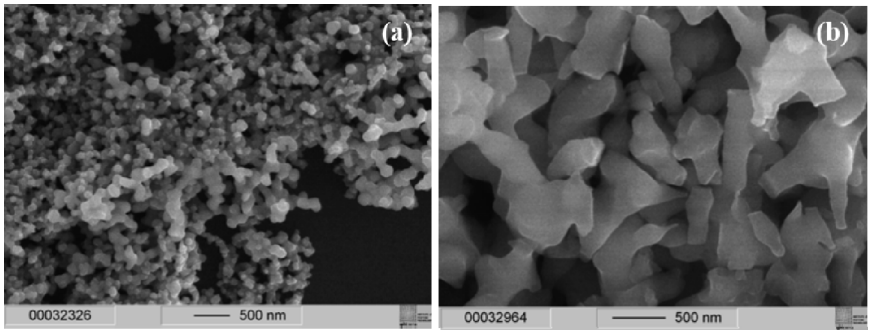


**Fig. 2.** SEM micrograph of unsintered (a) and presintered (b) P-doped silica soot material after a treatment with water ($xPOCl_3/xSiCl_4 = 0.3$, $T_{pre} = 1085$ °C, oxygen atmosphere).

Figure 2 illustrates the different morphology of unsintered (highest porosity) and presintered P-doped soot material after water treatment and subsequent drying, in analogy to the solution

Optical Materials EXPRESS

doping procedure. As observed for the soot material without water treatment, the unsintered material exhibits more spherical randomly ordered morphology, whereas the presintered material appears more densified. Furthermore, comparing the soot without and with water treatment, only a small morphological change in case of the unsintered soot with respect to geometry is visible: The round randomly crosslinked particles of unsintered soot seem to be stronger separated because some of material disappears by the water treatment.

### 3.2. EDX-Analysis

EDX analysis was performed in order to determine the chemical composition of the different soot materials. The obtained P-concentrations are summarized at Table 1.

**Table 1. Phosphorus concentration $cP_2O_5$ of P-doped silica soot material as a function of atmosphere during the presintering step**

| $xPOCl_3$ / $xSiCl_4$ = 0.3 (series A) | | | | $xPOCl_3$ / $xSiCl_4$ = 0.6 (series B) | | | |
|---|---|---|---|---|---|---|---|
| $T_{pre}$ | $V_{pre}$ | $\varphi_{rel}$ | $cP_2O_5$ | $T_{pre}$ | $V_{pre}$ | $\varphi_{rel}$ | $cP_2O_5$ |
| [°C] | [sccm] | | [mol%] | [°C] | [sccm] | | [mol%] |
| - | unsintered | 0.05 | 9.9 | - | unsintered | 0.04 | 11.7 |
| 1100 | 200 $O_2$ | 0.23 | 7.2 | 1050 | 200 $O_2$ | 0.23 | 9.0 |
| 1100 | 200 He | 0.19 | 6.6 | 1050 | 200 He | 0.16 | 7,9 |
| 1085 | remaining $O_2$ | 0.12 | 8.4 | 1000 | remaining $O_2$ | 0.17 | 10.8 |

Increasing the ratio of $xPOCl_3$ /$xSiCl_4$ by a factor of two leads to a slight increase in P-content e.g. from 9.9 mol% to 11.7 mol% $P_2O_5$ in case of the unsintered soot. Due to thermodynamics of deposition and side reactions, P incorporation during MCVD process is limited. Also, presintered soot contains less P species than unsintered soot, which is attributed to thermally induced evaporation losses during presintering.

Apparently, gas flow $V_{pre}$ during presintering affects the P-content in the porous soot. The P-contents decrease in the order unsintered > sintering under remaining oxygen (no gas flow during presintering) > 200 sccm oxygen > 200 sccm helium, corresponding with the increasing heat conductivity of the presintering atmosphere. Comparing He to $O_2$, its higher heat conductivity leads to an increased heat transmission within the soot layer thus creating higher temperatures within the soot material. That's why it is assumed that in case of helium the effective temperature achieved within the soot layer during presintering is in highest for the four different conditions under consideration. Likewise, the obtained relative density is estimated to be in general the highest in reverse order of the P-content. This assumption could be verified by microscopic analysis as described above.

The impact of relative density $\varphi_{rel}$ (reflecting the effective presintering temperature $T_{pre}$) on the phosphorus concentration $cP_2O_5$ of the soot material of series A and B is illustrated in Fig. 3 and Table 2. An increased $\varphi_{rel}$ (resp. $T_{pre}$) decreases the phosphorus concentration. The increase is more pronounced for $\varphi_{rel} < 0.1$, whereas it levels off for $\varphi_{rel} > 0.1$. Note, that at low $\varphi_{rel}$ a higher measurement error for $P_2O_5$ has to be taken into account.

Besides the relative density, the atmosphere within the process tube during presintering has an effect on thermodynamic equilibrium of P-deposition and side reactions. During any thermal treatment, the condensed phase $P_2O_5$ is in equilibrium with volatile P oxides ($P_4O_{10}$, $P_4O_6$, $PO_2$, PO) [7]. Any gas flow will shift the equilibria towards the volatile specimen by steadily removing them, thus is constantly lowering the amount of condensed phase $P_2O_5$. However, under stationary condition, which is without any gas flow, only a very small to negligible gas flow is induced by the heat gradient along the tube which only slightly reduces the $P_2O_5$ level of the porous soot material. Therefore the presintering of the P-doped silica layer without any gas flow enables the highest phosphorus concentration. During analysis of the unsintered soot

Optical Materials EXPRESS

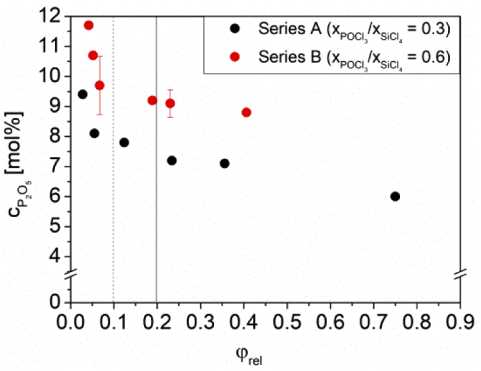


**Fig. 3.** Phosphorus concentration $cP_2O_5$ as a function of relative density $\varphi_{rel}$ of P-doped silica soot material of series A and B.

**Table 2. Phosphorus concentration $cP_2O_5$ of P-doped silica soot material as a function of presintering temperature**

| $xPOCl_3$ / $xSiCl_4$ = 0.3 (series A) [16] | | | | $xPOCl_3$ / $xSiCl_4$ = 0.6 (series B) | | | |
|---|---|---|---|---|---|---|---|
| $T_{pre}$ | $V_{pre}$ | $\varphi_{rel}$ | $cP_2O_5$ | $T_{pre}$ | $V_{pre}$ | $\varphi_{rel}$ | $cP_2O_5$ |
| [°C] | [sccm] | | [mol%] | [°C] | [sccm] | | [mol%] |
| - | unsintered | 0.05 | 9.9 | - | unsintered | 0.04 | 11.7 |
| 950 | 200 $O_2$ | 0.06 | 8.1 | 950 | 200 $O_2$ | 0.05 | 10.7 |
| 1050 | 200 $O_2$ | 0.12 | 7.8 | 1000 | 200 $O_2$ | 0.07 | 9.7 |
| 1100 | 200 $O_2$ | 0.23 | 7.2 | 1025 | 200 $O_2$ | 0.19 | 9.2 |
| 1135 | 200 $O_2$ | 0.36 | 7.1 | 1050 | 200 $O_2$ | 0.23 | 9.1 |
| 1175 | 200 $O_2$ | 0.75 | 6.0 | 1075 | 200 $O_2$ | 0.41 | 8.8 |

samples, a strong hygroscopic behavior was observed. Water uptake by P-doped, unsintered soot samples might lead to dissolution of deposited $P_2O_5$ according to

$$P_2O_5 + 3\ H_2O \rightarrow 2\ H_3PO_4$$

thus lowering the observed P-content. To exclude any measurement uncertainty caused by water uptake, P-doped soot samples were prepared at various $xPOCl_3/xSiCl_4$ ratios and analyzed before and after water treatment. The results are summarized in Table 3. In case of unsintered material, the phosphorus concentration after water treatment amounts around one-third of the concentration without water treatment. Presintering, on the other hand, is effective in preventing P-losses due to water treatment.

Due to the additional thermal presintering of the unsintered P-doped silica soot layer ($xPOCl_3/xSiCl_4 = 0.9$) and related evaporation side reactions, the phosphorus concentration is decreased from $cP_2O_5 = 13.6$ mol% down to 10.2 mol%. However, presintered soot is inert against water treatment. The water could not wash out the P-species in the presintered soot ($cP_2O_5 = 10.0$ mol%) like in unsintered soot material ($cP_2O_5 = 4.9$ mol%).

### *3.3. FTIR-Investigations*

#### 3.3.1. General

To our knowledge, an extensive FTIR band analysis of P-doped silica soot material obtained during MCVD process had been presented for the first time in [16]. Analysis of the IR-spectra allows to access the phosphorus concentration and the bonding of the P-atoms. One key aspect

Optical Materials EXPRESS

**Table 3. $cP_2O_5$ of unsintered and presintered P-doped silica soot material (series C) before and after water treatment as a function of deposition gas phase composition $xPOCl_3/xSiCl_4$**

| before water treatment [16] | | | after water treatment | |
|---|---|---|---|---|
| $xPOCl_3/xSiCl_4$ | $T_{pre}$ | $cP_2O_5$ | $cP_2O_5$ | c(after)/c(before) |
| | [°C] | [mol%] | [mol%] | [%] |
| 0.1 | unsintered | 4.3 | 1.2 | 30 |
| 0.2 | unsintered | 8.4 | 1.1 | 13 |
| 0.3 | unsintered | 9.7 | 3.0 | 31 |
| 0.4 | unsintered | 10.3 | 3.7 | 36 |
| 0.6 | unsintered | 11.0 | 3.4 | 31 |
| 0.9 | unsintered | 13.6 | 4.9 | 36 |
| 0.9 | 1000 | 10.2 | 10.0 | 98 |

in only the IR-spectra of unsintered soot samples was the observation of an additional band at 900 $cm^{-1}$ which so far could not be attributed to a known species in [16]. On the other hand, intense bands between 3700 - 1500 $cm^{-1}$ are clearly attributable to OH-vibrations of unsintered soot.

The main phosphorus related IR-bands of the soot are only registered in a wavenumber region of 1400–700 $cm^{-1}$. Here the overlap with IR-bands of silica makes it difficult to distinguish between the different P-bands (Table 4).

**Table 4. Characteristic IR wavenumbers of P-doped $SiO_2$ glass**

| Vibration Mode | Wavenumber | Reference |
|---|---|---|
| | [$cm^{-1}$] | |
| Si–O–Si asymmetric stretching | 1180 / 1060 | [10,11] |
| Si–O–Si symmetric stretching | 800 | [10,11] |
| P = O | 1325 | [12–15] |
| P-O-Si | 1100 | [13] |
| P-O-P | 1020 / 790 | [13] |

The morphology of both unsintered and presintered samples differs strongly which in turn influences the pressing of the thin soot layer on the ATR-diamond and thereby the sample contact. Consequently, the absorbance level of the unsintered and presintered soot material changes drastically. Figure 4 shows the IR-spectra of unsintered and presintered soot material ($T_{pre}$ = 1000 °C, $xPOCl_3/xSiCl_4$ = 0.9, oxygen atmosphere) in comparison to orthophosphoric acid (85%).

It illustrates that the band structure between 3700 - 1500 $cm^{-1}$ as well as the band at around 900 $cm^{-1}$ originate from acid and not from deposited soot itself. The measured IR-spectra of unsintered P-doped soot are an overlay of bands of $H_3PO_4$ and P-doped silica soot material itself.

In the following, the bands within the region 1400 $cm^{-1}$ - 700 $cm^{-1}$ will be assigned and discussed as a function of soot material. The difference of the spectra of an undoped silica soot reference and un- or presintered P-doped soot allows a band assignment (Fig. 5). As a result, the P = O-band at around 1325 $cm^{-1}$ and the P-O-Si-band at around 1100 $cm^{-1}$ are obviously more intense in the spectrum of the presintered soot. The unsintered soot spectrum displays a higher absorbance at the P-O-P-band at around 1000 $cm^{-1}$ and at a band at around 900 $cm^{-1}$ which is attributed to the formation of $H_3PO_4$.

The comparatively low value of P = O-band in the unsintered soot material in spite of the overall high phosphorus concentration and the generation of P = O-bonds during the presintering

Optical Materials EXPRESS

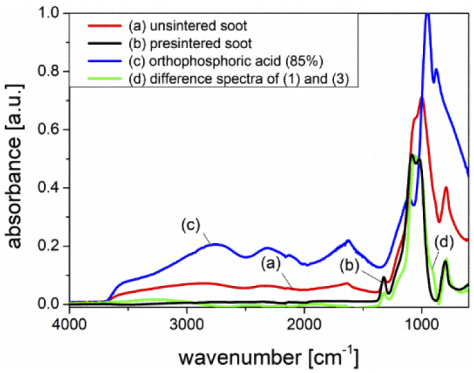


**Fig. 4.** Comparison of unsintered soot (a), presintered soot (b), orthophosphoric acid (c) and the difference spectra of orthophosphoric acid (85%) and unsintered soot (d).

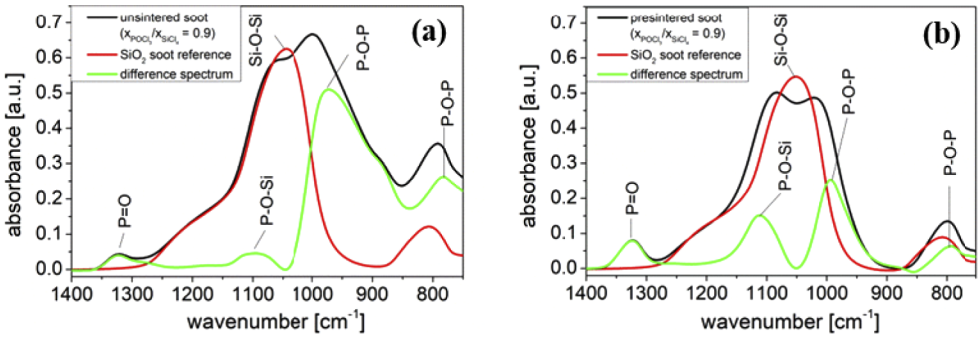


**Fig. 5.** IR-spectra of the unsintered (a) and presintered (b) P-doped soot material (both black lines), undoped silica soot reference (red line) and the difference spectra of both (green line).

indicate strong differences of the present P-species in the soot material. Hence, the presintering represents an important process step to control not only the relative density of the doped soot material, but also the achievable phosphorus concentration as well as the nature of the P specimen.

### 3.3.2. Influence of presintering atmosphere

The IR-spectra of the soot samples of series A and B (Fig. 6) illustrate the difference caused by the variation of the gas flow during presintering. The spectrum of the sample presintered under He flow shows the lowest absorbance level. The P = O-band (1325 $cm^{-1}$) and the P-O-P-band (~1000 $cm^{-1}$) are reduced evidencing a lower $cP_2O_5$ level that is attributed to stronger evaporation of the P-species with a helium flow during the presintering.

The spectral region between 950–1150 $cm^{-1}$ of the presintered samples under $O_2$ flow and under stationary conditions (without any flow) looks similar. Slight differences are observed for the P-O-Si and P-O-P band intensities. In case of stationary conditions, the P-O-P band is more pronounced than the P-O-Si (and vice versa for the $O_2$ flow condition). This is explained by reduced evaporation of the volatile P-species, so more P-O-P-bonds remain. The relative decrease of the P-O-Si-band intensity is an indication for the higher porosity of the soot (i.e. lower relative density) and so less P-O-Si-bonds. In contrast, the intensity of the P = O-band is similar or slightly increased in case of the presintering without any gas flow.

Thus the IR spectral analysis of the presintered and unsintered soot material has proven that the gas flow or the atmosphere during the presintering of a porous P-doped silica soot layer affects the

Optical Materials EXPRESS

phosphorus concentration and the P-species which are incorporated in the soot material. Without any gas flow during the presintering step of the MCVD process in combination with solution doping it is possible to achieve higher phosphorus concentrations in the soot.

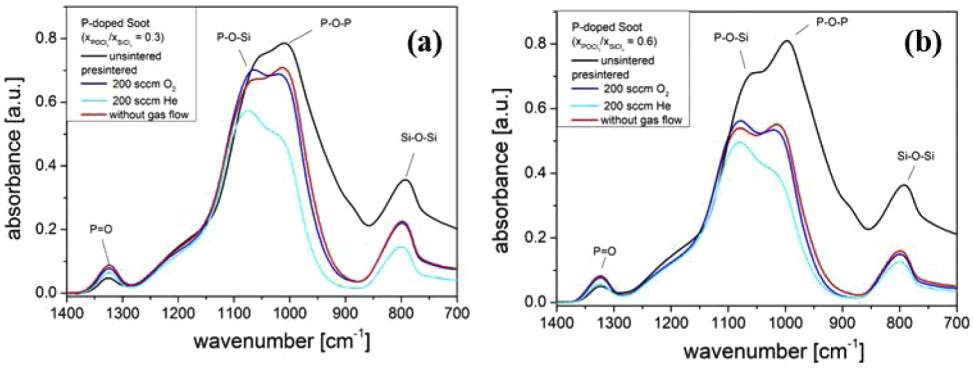


**Fig. 6.** IR-spectra of samples with different gas atmospheric conditions during the presintering of the porous P-doped soot material: unsintered, presintered under 200 sccm $O_2$, 200 sccm He, without gas flow.(a): $xPOCl_3$ / $xSiCl_4 = 0.3$; (b): $xPOCl_3$ / $xSiCl_4 = 0.6$)

### 3.3.3. Influence of water treatment

Another evidence for the difference of the unsintered and presintered P-doped silica soot material could be observed by the FTIR measurement of the soot before and after the water treatment (Fig. 7). While the spectrum of the presintered soot is only slightly affected at a wavenumber of around 1000 $cm^{-1}$ (P-O-P-band), the spectrum of the unsintered material after water treatment is strongly changed. A significant lower amount of P-O-P-bonds and a slightly reduced P = O-band intensity are observed. Hence, it is concluded that the unsintered soot material consists mainly of P-species with numerous P-O-P-units without chemically bonding to the silica matrix.

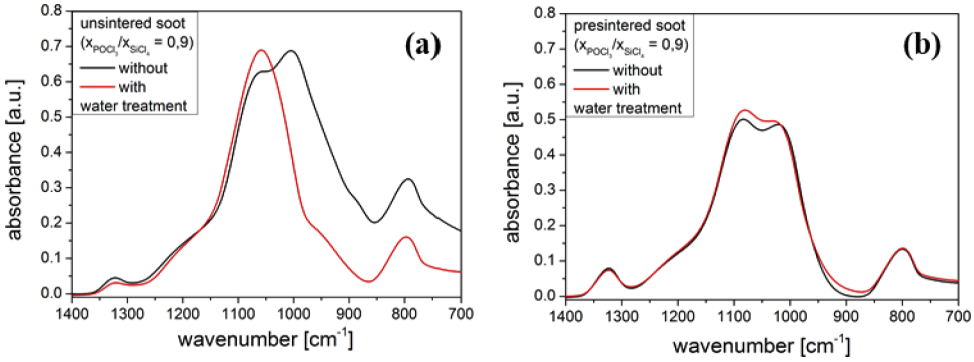


**Fig. 7.** IR-spectra of unsintered (a) and presintered (b) P-doped silica soot material before and after a treatment with an aqueous solution.

According to [16] the overall $P_2O_5$ concentration of the soot material can be estimated from the ratio of the areas of the P = O-band (1325 $cm^{-1}$) and the Si-O-Si-band (800 $cm^{-1}$), that is the phosphorus band area ratio (PBAR). This was done for the comparison of the effects of water treatment, and the results are plotted against the WDX measured phosphorus concentration (Fig. 8). There is a good agreement in the trend of both types of analysis.

Optical Materials EXPRESS

The reduced numbers of P-species with P-O-P-bonds enable a good agreement of both measurements in case of the unsintered soot material after the water treatment. This indicates that the remaining P-species have P = O- and P-O-Si-bonds and are strongly linked to the silica network. The similar PBAR value before and after water treatment illustrates, that the P-species with P = O-bonds are not affected by the water.

The presintering of the porous P-doped silica soot layer leads to the formation of more P = O- and P-O-Si-bonds and therefore to a stronger connection of the incorporated P-species into the silica network. This temperature treatment is also important to achieve a specific relative density and to enable an efficient incorporation of RE or Al. During the solution doping procedure the Al- or RE-ions interact with the porous P-doped silica matrix. Here the P = O-bonds seems to be important for the incorporation of the dopants. For example during the formation of $AlPO_4$-tetrahedra the Al-ions enter the matrix at the P = O-bond position and this leads to a change of the valence of P from $P^{5+}$ to $P^{4+}$ and Al from $Al^{3+}$ to $Al^{4+}$ [17,18]. An increased number of P = O-bonds in the porous P-doped silica material should then improve the Al incorporation. This topic is still under investigation.

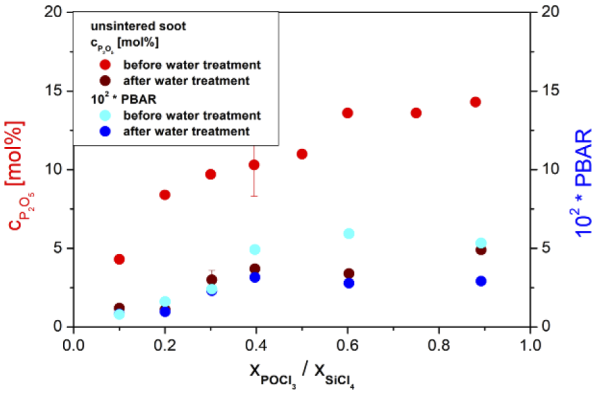


**Fig. 8.** Phosphorus concentration $cP_2O_5$ and phosphorus band area ratio (PBAR) of unsintered P-doped silica soot material before and after a treatment with an aqueous solution.

## 4. Conclusion

In this paper spectroscopic and morphological investigations of porous P-doped silica soot material as a function of process parameters (e.g. starting gas phase composition for porous layer deposition, gas flow and atmosphere during presintering, aqueous solution soaking) are described. The reverse deposition of the porous unsintered soot layer, the presintering of this layer and the soaking of both layer types generates differences in the morphology. The strongest morphological changes which are caused by presintering, include the flattening and aggregation of spherical structures to denser structures that adheres stronger to the surface of the substrate tube.

Porosity and P-content of the soot layer depend on presintering temperature as well as on the starting gas phase composition used for porous layer deposition. Especially, a reduction of the phosphorus concentration after the presintering step was observed which is ascribed to the thermodynamically induced generation of volatile P-species. In absence of gas flow during the presintering step, a 10% higher phosphorus concentration of the silica soot material in comparison to the conventional treatment was achieved. The water treatment (being representative for solution doping step) in case of unsintered soot material causes the strongest decrease of the P-concentration up to one-thirds of the origin concentration.

Optical Materials EXPRESS

The unsintered soot layer was found to consist of P-species with mainly P-O-P-bonds and few P-O-Si- and P = O-bonds. Presintering of this soot material causes morphological changes, increases its specific relative density while at the same time the P-content decreases and more P-O-Si and P = O-bonds are generated within the soot. The reduction of P-content is reflected by the apparent decrease of P-species consisting of P-O-P bonds rather than those with P = O- and P-O-Si. Obviously, the P-species which are bonded directly to the silica network are more stable towards solution or temperature treatment.

In order to achieve higher phosphorus concentrations, a relative density $\varphi_{rel}$ of the porous soot layer should be adjusted to values slightly lower than 0.2. This enables to limit the phosphorus evaporation and, at the same time, to ensure good adhesion of the deposit to the substrate tube by generating a maximum of P-species with more P = O- and P-O-Si-bonds. This value seems to be important for an efficient incorporation of the RE and Al via solution doping. It can be individually tuned, but one has to keep in mind to mitigate P concentration, porosity and layer adhesion. For P-doped silica soot material of the MCVD process in combination with solution doping the P = O-bonds are an important indicator for the phosphorus concentration, the connection of the P-ions to the silica matrix and the interaction with the dopants of the solution.

## Acknowledgments

The authors are grateful for the financial support from the Leibniz Institute of Photonic Technology Jena and the helpful discussions with Dr. F. Froehlich and Dr. S. Unger.

## Disclosures

The authors declare no conflicts of interest.

## References

1. S. Unger, A. Schwuchow, S. Jetschke, V. Reichel, A. Scheffel, and J. Kirchhof, "Optical properties of Yb-doped laser fibers in dependence on codopants and preparation conditions," Proc. SPIE **6890**, 689016 (2008).
2. S. Unger, A. Schwuchow, S. Jetschke, V. Reichel, M. Leich, A. Scheffel, and J. Kirchhof, "Influence of aluminium-phosphorus codoping on optical properties of ytterbium-doped laser fiber," Proc. SPIE **7212**, 72121B (2009).
3. S. Jetschke, S. Unger, A. Schwuchow, M. Leich, and J. Kirchhof, "Efficient Yb laser fibers with low photodarkening by optimization of the core composition," Opt. Express **16**(20), 15540–15545 (2008).
4. J. E. Townsend, S. B. Poole, and D. N. Payne, "Solution-doping technique for fabrication of rare-earth-doped optical fibres," Electron. Lett. **23**(7), 329–331 (1987).
5. J. Kirchhof, S. Unger, and A. Schwuchow, "Fiber Lasers: Materials, Structures and Technologies," Proc. SPIE **4957**, 1 (2003).
6. J. Kirchhof, S. Unger, A. Schwuchow, S. Grimm, and V. Reichel, "Materials for high-power fiber lasers," J. Non-Cryst. Solids **352**(23-25), 2399–2403 (2006).
7. J. Kirchhof, S. Unger, A. Schwuchow, S. Jetschke, and B. Knappe, "Spatial distribution effects and laser efficiency in Er/Yb doped fibers," Proc. SPIE **5350**, 222 (2004).
8. D. J. DiGiovanni, T. F. Morse, and J. W. Cipolla Jr, "Theoretical Model of Phosphorus Incorporation in Silica in Modified Chemical Vapor Deposition," J. Am. Ceram. Soc. **71**(11), 914–923 (1988).
9. R. Youngman, C. Hogue, and B. Aitken, "Crystallization of Silicon Pyrophosphate from Silicophosphate Glasses as Monitored by Multi-Nuclear NMR," Mater. Res. Soc. Symp. Proc. **984**, 0984-MM12-03 (2006).
10. M. Handke, W. Mozgawa, and M. Nocun, "Specific features of the IR spectra of silicate glasses," J. Mol. Struct. **325**, 129–136 (1994).
11. N. Shibata, M. Horigudhi, and T. Edahiro, "Raman spectra of binary high-silica glasses and fibers containing $GeO_2$, $P_2O_5$ and $B_2O_3$," J. Non-Cryst. Solids **45**(1), 115–126 (1981).
12. J. Wong, "Vibrational spectra of vapor-deposited binary phosphosilicate glasses," J. Non-Cryst. Solids **20**(1), 83–100 (1976).
13. V. G. Plotnichenko, V. O. Sokolov, V. V. Klotashev, and E. M. Dianov, "On the structure of phosphosilicate glasses," J. Non-Cryst. Solids **306**(3), 209–226 (2002).
14. C. Dayanand, G. Bhikshamaiah, V. Jaya Tyagaraju, M. Salagram, and A. S. R. Krishna Murthy, "Structural investigations of phosphate glasses: a detailed infrared study of the x(PbO)-(1-x)$P_2O_5$ vitreous system," J. Mater. Sci. **31**(8), 1945–1967 (1996).
15. D. E. C. Corbridge and E. J. Lowe, "Infrared spectra of some inorganic phosphorus compounds," J. Chem. Soc. **23**(6), 493–502 (1954).

Optical Materials EXPRESS

16. F. Lindner, S. Unger, A. Kriltz, A. Scheffel, A. Dellith, J. Dellith, and H. Bartelt, "Phosphorus incorporation into silica during modified chemical vapor deposition combined with solution doping," Phys. Chem. Glasses: Eur. J. Glass Sci. Technol., Part B **56**(6), 278–284 (2015).
17. M. Rokita, M. Handke, and W. Mozgawa, "Spectroscopic studies of the amorphous $SiO_2$–$AlPO_4$ materials," J. Mol. Struct. **511-512**, 277–280 (1999).
18. S. G. Kosinski, D. M. Krol, T. M. Duncan, D. C. Douglas, J. B. MacChesney, and J. R. Simpson, "Raman and NMR spectroscopy of SiO2 glasses co-doped with $Al_2O_3$ and $P_2O_5$," J. Non-Cryst. Solids **105**(1-2), 45–52 (1988).